IEEE Access
Multidisciplinary | Rapid Review | Open Access Journal

Received August 6, 2021, accepted August 23, 2021, date of publication August 25, 2021, date of current version September 2, 2021.

Digital Object Identifier 10.1109/ACCESS.2021.3107904

Total Variant Based Average Sparsity Model With Reweighted Analysis for Compressive Sensing of Computed Tomography

TARIQ RAHIM[1], (Member, IEEE), LEDYA NOVAMIZANTI[2], (Graduate Student Member, IEEE), I NYOMAN APRAZ RAMATRYANA[1], (Graduate Student Member, IEEE), SOO YOUNG SHIN[1], (Senior Member, IEEE), AND DONG SEONG KIM[1], (Senior Member, IEEE)

[1]Department of IT Convergence Engineering, Kumoh National Institute of Technology, Gumi 39177, Republic of Korea
[2]School of Electrical Engineering, Telkom University, Bandung 40257, Indonesia

Corresponding author: Dong Seong Kim (dskim@kumoh.ac.kr)

This work was supported in part by the Ministry of Science, ICT (MSIT), South Korea, through the Information Technology Research Center Support Program supervised by the Institute for Information Communications Technology Planning and Evaluation (IITP), under Grant IITP-2021-2020-0-01612, and in part by the Priority Research Centers Program through the National Research Foundation of Korea (NRF) through the Ministry of Education, Science and Technology under Grant 2018R1A6A1A03024003.

ABSTRACT Computed tomography (CT) in medical is an imaging procedure employed to generate detailed images of bones, soft tissue, internal organs, and blood vessels. However, prolonged acquisition time is yet a bottleneck that can lead to patient discomfort in addition to the cost constrain and exposure to X-rays used by CT. In medical imaging technologies and implementations, effective sampling and transmission techniques are some of the main areas of study to overcome such problems. To fulfill this requirement, the compressive sensing (CS) technique was introduced demonstrating that such compression is possible and can be accomplished throughout the process of data restoration; and that the uncompressed frames can be recovered employing a scalable approach of computational optimization. Sparsity averaging reweighted analysis (SARA) was proposed in compressed imaging, exploiting multi-basis sparsity with averaging approach and basis pursuit denoise (BPDN) with high signal to noise (SNR) results. In SARA, the processing time is not considered due to the high processing time because of iteration in the reweighted process and it is not feasible for the medical image that needs fast processing with high SNR result. To fulfill this gap, this paper proposes total variation based average sparsity model with reweighted analysis for CT imaging. The SNR, structural similarity index (SSIM), and processing time are used as performance metrics for the comparison of the proposed and existing techniques. From detailed experimental results, the proposed technique outperforms the existing CS techniques and is considered as a feasible solution for compressed sensing (CS) based CT images compression with faster delay process and better visual quality for medical images.

INDEX TERMS Average sparsity model, compressive sensing, CT images, SARA, SNR, SSIM, total variation (TV).

I. INTRODUCTION

Computed tomography (CT) scans are employed to perform a very significant role in disease diagnosis and surgical planning. CT was introduced as an alternative tool designed to help physicians in the examination of multiple diseases. Those tools utilize analysis of the data to evaluate the condition of the patient [1]. Nevertheless, by its characteristics, exposure to high X-ray radiations of CT scans and prolonged acquisition time is yet a bottleneck that can lead to patient discomfort and lifetime risk of cancer [2]. Another dilemma related to CT images is the storage of the large size of the image file and transmission. For instance, a total of 150 MB size of an image file size of 512 × 512 encoded at 16-bit

The associate editor coordinating the review of this manuscript and approving it for publication was Hengyong Yu.

is reported for a data set comprised of 200 to 400 image files. Managing such data is a hard task, therefore; data must correspond to high-quality standards to guarantee that the clinical data is accurate and reliable. Effective data compression techniques can help in the mitigation of these issues [3].

Compressive sensing (CS) provides a sampling structure for a signal below the Nyquist sampling rate principle for retrieving signal from a compressed amount of samples [4]–[6]. By utilizing the CS method, simultaneous sampling and compression of sparse signals are performed, and the sparse signals can be reconstructed from compressed signal in measurements process [7]. CS is approved by the U.S. Food and Drug Administration and employed for taking the advantage both in terms of speed and quality for the diagnosis cases [8]. Furthermore, in the CS techniques, there is no need for adjacent approximation within the image characteristic and sampling pattern, i.e, medical imaging data. Medical imaging data such as CT where prolonged acquisition time is yet a bottleneck that can lead to patient discomfort in addition to the cost constrain and exposure to dangerous X-rays [9].

Previously, sparsity averaging was proposed in natural images considering CS with coherent dictionaries and the relevant algorithm is also based on the analysis of reweighted ℓ_1 formulations, which is labeled as Sparsity Averaging Reweighted Analysis (SARA) [10]. SARA is further enhanced by multi-basis sparsity averaging (M-BRA) for 4-data medical images [11]. In M-BRA, SSIM and processing time are considered. In medical imaging, processing time is a critical issues and not considered in [10]. SARA is compared with Haar type wavelet with reweighted analysis (RW-Haar), Daubechies wavelet with reweighted analysis (RW-Db), curvelet with reweighted analysis (RW-Curvelet), and total variant with reweighted analysis (RW-TV). RW-TV is a simple reconstruction method with less iteration compared to SARA and a good comparison for SARA in the view of processing time.

Motivated by the above discussion, total variant based average sparsity model with reweighted analysis is proposed for CT imaging. For CT image compression based on CS, the signal to noise (SNR), structural similarity index (SSIM), and processing time are employed as performance metrics. The followings are the main contributions of the paper:

- A detailed comparative analysis of the CS method for reconstruction in CT images filling the gap for medical imaging, we have investigated the proposed CS technique that is benchmarked with average sparsity model, Haar, and Curvelet.
- The performance of the proposed and the existing CS technique is investigated in terms of performance metrics such as SNR, SSIM, and processing time that was lacking in the previous studies. Evaluation of its resulted in filling the gap of reconstruction of medical image analysis such as CT.
- Based on the experimental results, detailed results are provided in this study showing that the proposed approach as CS technique outperformed the SARA technique in terms of better SNR and lesser processing time for reconstruction.

II. RELATED WORK

Recently, CS offered observations both in terms of engineering application aspects and theoretical aspects [7]. Distinguished from other compressing methods, CS promotes an advantage in an area like slower sampling conditions, especially when dealing with medical data such as CT. Here in CT data where prolonged acquisition time is yet a bottleneck, a slower sampling rate is considered as a significant disadvantage. Research work has been performed while employing the CS methods for the reconstruction of CT image based on sampling strategy and sparse-view [12]–[14]. Approximate message passing (AMP) methods outline the popularity for determining under-sampling CS dilemmas with arbitrary linear estimations, but there are yet no explicit explications on how AMP can operate with real-world obstacles. AMP is employed for CT imaging of sparse nature where the reconstruction is achieved by performing modification within AMP yielding into an algorithm i.e., denoising generalized approximate message passing CT. This modification is in terms of the design of a reliable preconditioner for the method depends on the forward estimation model along with the Poisson nonlinear noise model [15]. Based on CS works, a repetitive algorithm is developed for the total variation (TV) minimization of the image subjected to the restriction that the computed projected image lies in between a particularized threshold of the prepared image. The TV-based approach which utilizes sparseness has proven its capacity in the reconstruction of CT images despite smoothing of the image can result in lessening the spatial resolution and contrast of the image [16]. The sparsity view CT restoration problem is coped with a minimization composite restoration framework that combines the wavelet frame to TV. This composite model employs the low-frequency wavelet image coefficients TV-norm and high-frequency wavelet image coefficients of ℓ_0 norm for eliminating the staircase effect and providing smooth regularization [17]. Wavelet packet extensions have been the focus of various research enigmas in the last several years. Approximation of the $L^2(\mathbb{R})$ employing wavelet packets for different transforms such as Hilbert and Hartley-like is investigated [18], [19]. For image restoration, a prior information regularization method and reweighted TV (RTV-PIR) is presented. The RTV-PIR is based on the TV the minimization for miss-computed as wall structures [20]. Prior discriminative information based joint evaluation structure named discriminative prior-prior image restrained CS method is presented for the reconstruction of low dose CT image [21]. A Radon transform based on fast pseudo polar Fourier transform is proposed for lessening the computational restrictions and processing time for CT images. The maximum-a-posterior approach has opted for the analysis of the restoration process [22]. Furthermore, a deterministic measurement matrix is formed for the reconstruction of the original signal from the compressed representations without the information of

the order of sparsity [23]. Employing smoothed ℓ_o norm as a reconstruction method [24], high-quality images are reconstructed from CS measurements.

Deep learning (DL) approaches are extensively explored for the CS techniques to reconstruct images in an efficient manner [25]. Two versions of the unique DL model, entitled as ADMM-CSNet are proposed that integrate the conventional model-based CS approach and data-driven DL approach for the reconstruction of the image from sparsely sampled measures [26]. A multi-scale deep compressive imaging that simultaneously acquires to disintegrate, sample, and restore images at multi-scale is proposed. The framework is a three-stage end-to-end training system where the primary two stages are employed for the reconstruction followed by the performance enhancement stage [27]. Furthermore, a two-branch convolution residual network that is comprised of a two-branch convolution auto-encoder network and a residual network is proposed for CS [28]. Moreover, generative adversarial neural networks are explored in detail manner for the reconstruction of images as CS approaches [29], [30].

Sparsity Averaging Reweighted Analysis (SARA) was introduced for restoration considering radio-interferometric images employing Fourier imaging [10]. Moreover, SARA was examined employing natural images with redundant dictionaries that are coherent [31]. In our previous work, a detailed investigation of using the enhanced form of the SARA method using a varying number of frames and unique wavelet basis for medical data such as colonoscopy, endoscopy, and MRI was performed. However, we move to step ahead for the examination of CT images which are evaluated to fill the gap in the lack of SARA evaluation in medical images and compared to the reweighted total variation (RW-TV) [11].

III. METHODOLOGY

The proposed CS technique has an average sparsity model to generate sparsity averaging and a reweighted analysis to update the weight for TV reconstruction method. This architecture is illustrated in Fig. 1. To obtain the prepared image, the original CT image is processed within the data preparation stage. The preparation starts with the data processing as described in section IV-A followed by the spread-spectrum (SS) [32] analysis for the CS measurements to obtain the compressed or measured vector. Then, for the average sparsity model as detailed in section III-A, generation of a sparsity averaging basis is performed. Furthermore, this work only concentrating on basis pursuit denoise (BPDN) and TV approach for the CS restoration that is practiced in the early research work for benchmarking purposes. Lastly, a reweighted analysis is conducted for convex optimization that is described in section III-B.

A. AVERAGE SPARSITY MODEL

Considering a CT image with $n \times n$ pixels denoted as $\boldsymbol{I} \in \mathbb{R}^{n\times n}$ and reshaped to one dimension signal (1D) $\boldsymbol{s} \in \mathbb{R}^{N\times 1}$ where $N = n \times n$. Then, $\boldsymbol{s}$ is transformed by Fourier transform in a way of complex-valued as $\boldsymbol{x} \in \mathbb{C}^{N\times 1}$, where $\boldsymbol{x}$ denotes sparse signal according to an $\boldsymbol{\Psi} \in \mathbb{C}^{N\times N}$ orthonormal basis. Here, the signal $\boldsymbol{x}$ is represented by a sparse transform basis $\boldsymbol{s}$, i.e., $\boldsymbol{x} = \boldsymbol{\Psi s}$ for $\boldsymbol{s} \in \mathbb{C}^{N\times 1}$. Moreover, the measurement vector method $\boldsymbol{y} \in \mathbb{C}^{M}$ is modeled by $\boldsymbol{y} = \boldsymbol{\Phi x}$, where $\boldsymbol{\Phi} \in \mathbb{C}^{M\times N}$ with $M < N$ denotes a measurement matrix.

A conventional approach for recovering s from y is a convex problem subjected to $\min_{\bar{\boldsymbol{s}}\in\mathbb{C}^M} \|\boldsymbol{s}\|_1$ and limited to $\|\boldsymbol{y} - \boldsymbol{\Phi\Psi}\bar{\boldsymbol{s}}\|_2 \leq \varepsilon$, where $\|\cdot\|_1$ is ℓ_1 norm and ε is the upper bound of ℓ_2 norm. The recovered signal is denoted by $\hat{\boldsymbol{x}} = \boldsymbol{\Psi}\hat{\boldsymbol{s}}$ where $\hat{\boldsymbol{s}}$ is the solution for the convex problem declared above, named as a synthesis based problem. In [4], $\boldsymbol{\Psi}$ and $\boldsymbol{\Phi}$ are needed to be orthonormal according to a restricted isometry property (RIP).

CS can be represented as multiple dictionaries with sparsity basis $\boldsymbol{\Psi} \in \mathbb{C}^{N\times D}$ having $N < D$, $\boldsymbol{x} = \boldsymbol{\Psi s}$, and $\boldsymbol{s} \in \mathbb{C}^{D}$. To retrieve $\boldsymbol{s}$ as synthesis problem formulation having condition on $\boldsymbol{\Psi}$ that $\boldsymbol{\Phi\Psi}$ meet the requirements of RIP [33]. A theoretical approach where the signal determines the analysis for the problem of ℓ_1 norm investigation is performed [34], and is given as:

$$\min_{\bar{\boldsymbol{s}}\in\mathbb{C}^M} \left\|\boldsymbol{\Psi}^{\dagger}\bar{\boldsymbol{s}}\right\|_1 \quad \text{subject to } \|\boldsymbol{y} - \boldsymbol{\Phi}\bar{\boldsymbol{x}}\|_2 \leq \varepsilon, \tag{1}$$

where $\boldsymbol{\Psi}^{\dagger}$ indicates the ad-joint operator of $\boldsymbol{\Psi}$.

A CS approach is introduced named a SS framework with a sub-sampled Fourier matrix where the multiplication of the signal with a wide bandwidth modulation is performed. The outcomes are validated by a mathematical investigation of the state transition of the ℓ_1 minimization problem [32]. When $\boldsymbol{\Psi}$ and $\boldsymbol{\Phi}$ satisfy the basis of D-RIP along with the representation of all frames, then the answer to (1), expressed by $\hat{\boldsymbol{s}}$ satisfies the error threshold as follows:

$$\|\hat{\boldsymbol{s}} - \boldsymbol{s}\|_2 \leq C_0\varepsilon + C_1K^{-\frac{1}{2}}\left\|\boldsymbol{\Psi}^{\dagger}\boldsymbol{s} - \left(\boldsymbol{\Psi}^{\dagger}\boldsymbol{s}\right)_K\right\|_1, \tag{2}$$

where $\left(\boldsymbol{\Psi}^{\dagger}\boldsymbol{s}\right)_K$ indicates the fittest K-iteration approximation of $\boldsymbol{\Psi}^{\dagger}\boldsymbol{s}$ while C_0 and C_1 are constants. The Ω-RIP also reflected the same D-RIP characteristics resulting in the presentation of co-sparsity analysis model [35].

CT images are intricate and include multiple structures yielding sparse representations in multiple bases. A dictionary incorporating a concatenation of 8 Daubechies (Db) wavelet bases $\boldsymbol{\Psi}$ is expressed [31] by

$$\boldsymbol{\Psi} = \frac{1}{\sqrt{8}}\left[\boldsymbol{\Psi}_1, \boldsymbol{\Psi}_2, \ldots, \boldsymbol{\Psi}_8\right], \tag{3}$$

where $\boldsymbol{\Psi}_1$ denotes the first Daubechies (Db) wavelet basis and denoted as Db1, and so on $\boldsymbol{\Psi}_8$ denoted as Db8. The analysis-based formation is a fitting method for enhancing the average sparsity; consequently, the subsequent method is recommended that is equal to a new average sparsity model which is expressed by

$$\left\|\boldsymbol{\Psi}^{\dagger}\bar{\boldsymbol{x}}\right\|_0 = \sum_{f=1}^{8}\left\|\Psi_f^{\dagger}\bar{x}\right\|_0. \tag{4}$$

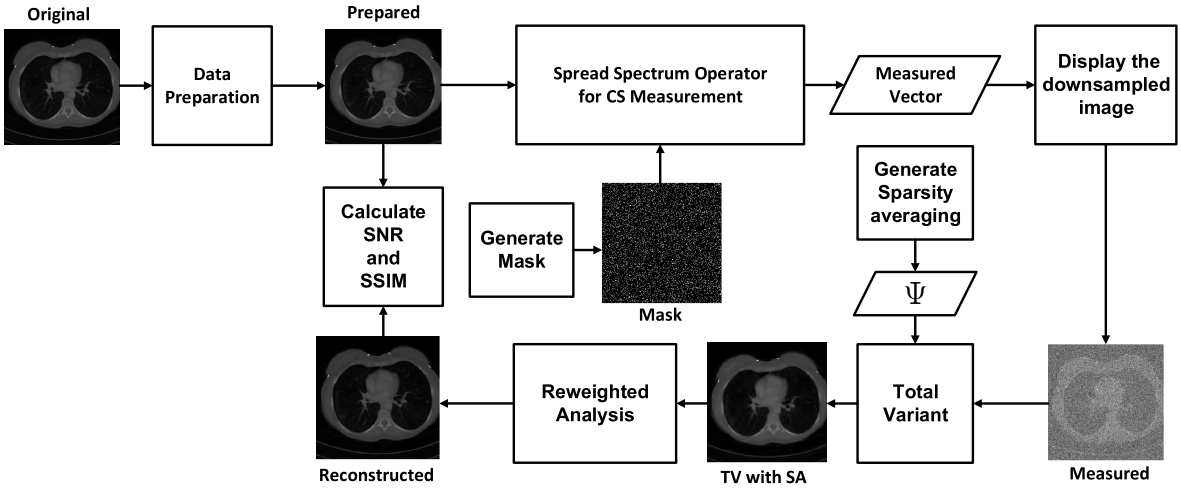

FIGURE 1. The proposed system model of CS-based CT medical image compression.

Every frame in this formation contains the complete knowledge of the signal, therefore a method of such nature cannot be represented in a synthesis-based frame. For multiple frames, prior investigations conceded a component separation approach that decomposes the signal as $\boldsymbol{x} = \sum_{f=1}^{8} \boldsymbol{x}_f$ where each segment $\boldsymbol{x}_f$ in the f_{th} basis is sparse [36], [37].

B. TV-SA WITH REWEIGHTED ANALYSIS

Algorithm 1 detail the approach of the proposed technique which initiates with average sparsity Ψ model construction process followed by the computation of a solution for TV γ_i^k employing (6). Then for enhancing the initial TV solution, the process of reweighted is conducted as a loop. The loop of the reweighting process is terminated subjected to the condition that the successive solutions are smaller than the restrained $\eta \in (0, 1)$, or the highest number of iterations, t_{max}, has been obtained.

TV is a typical regularizer that takes use of natural images with a piecewise smooth structure. In image, TV norm penalizes the presence of edges to achieve sparsity of image edges. Isotropic TV convention is applied, which a group $\ell_{2,1}$ sparsity penalty to penalize horizontal and vertical forward-differences jointly are used. For the example, $\|\boldsymbol{x}\|_{\mathrm{TV}} = \sum_{i=1}^{N} \|\boldsymbol{T}_i\boldsymbol{x}\|_2$, where $\boldsymbol{T}_i \in \mathbb{R}^{2\times N}$ denotes a TV matrix whose rows performs the extraction of the horizontal and vertical forward differences of the i^{th} pixel of $x \in \mathbb{R}^N$. Furthermore, reweighted TV (RW-TV) is commonly declared as an iterative algorithm:

$$\hat{\boldsymbol{x}}^{(k+1)} = \arg\min_{x\geq 0} \frac{1}{2}\|\boldsymbol{y} - \boldsymbol{M}\boldsymbol{A}\boldsymbol{x}\|_2^2 + \gamma_0 \sum_{i=1}^{N} \gamma_i^{(k)} \|\boldsymbol{T}_i\boldsymbol{x}\|_2 , \quad (5)$$

where the goal is to retrieve from measurements $y \in \mathbb{R}^M$, the underlying signal $x \in \mathbb{R}_+^N$ (e.g., a vectorized non-negative image), that has been linearly operated on by matrices

Algorithm 1 The Proposed Algorithm

Input: $\boldsymbol{y}$, $\boldsymbol{\Phi}$, β, η, σ_x, t_{max}, and ε
Output: Reconstructed image $\hat{\boldsymbol{x}}$
Construct average sparsity Ψ
Compute TV solution γ_i^k
Initialization $\rho = 1$, $t = 1$, $\upsilon^{(0)} = \sigma_x(\boldsymbol{\Psi}^\dagger\hat{\boldsymbol{x}}^{(0)})$, and $W^{(0)} = 1$;
while $t < t_{max}$ *and* $p > \eta$ **do**
  Weight matrix update $W_{ij}^{(t)} = f(\upsilon^{(t-1)}, \hat{\boldsymbol{x}}^{(t-1)})\delta_{ij}$, for $i, j = 1, \ldots, G$ with $\hat{\boldsymbol{x}}^{(t-1)} = \boldsymbol{\Psi}^\dagger\hat{\boldsymbol{x}}^{(t-1)}$;
  Compute a solution $\hat{\boldsymbol{x}}^{(t)} = \gamma_i^{(k+1)}$ with $W_{ij}^{(t)}$;
  Update $\upsilon^{(t)} = \max\left\{\beta\upsilon^{(t-1)}, \sigma_x\right\}$;
  Update $\rho = \frac{\left\|\hat{\boldsymbol{x}}^{(t)} - \hat{\boldsymbol{x}}^{(t-1)}\right\|_2}{\left\|\hat{\boldsymbol{x}}^{(t-1)}\right\|_2}$;
  $t \leftarrow t + 1$;
end

$\boldsymbol{A} \in \mathbb{R}^{N\times N}$ indicating a convolution operator (i.e., Toeplitz) and $M \in \{0, 1\}^{M\times N}$ representing a masking matrix whose rows are a subset of the rows (i.e., $M \leq N$) of an identity matrix defining the non-masked pixel support.

The parameter γ_0 refers to the TV regularization parameter while the individual weights γ_i are a function of $\left\|\boldsymbol{T}_i\hat{\boldsymbol{x}}^{(k)}\right\|_2$, i.e., the i^{th} weight

$$\gamma_i^{(k+1)} = \frac{1}{\left\|\boldsymbol{T}_i\hat{\boldsymbol{x}}^{(k)}\right\|_2 + \epsilon}, \quad (6)$$

includes the i^{th} edge of the previous iteration's estimation in its denominator, as well as a tiny positive constant ϵ to prevent weights from blowing out to infinity. Iteratively, active edges will be penalized less, encouraging them to be active, while inactive edges will be penalized more.

IV. EXPERIMENT

A. DATASET AND DATA PREPARATION

For an overarching CT image compression analysis of the patients who had head, neck, and lung cancer, L3 abdominal axial CT images were obtained [38]. The data set was acquired by one expert operator using Slice-O-Matic V4.3 software at the Cross Cancer Institute (CCI), University of Alberta, Canada. Total data of 100 images in a 512×512 pixels resolution DCM file format. The resolution of the CT images is recorded in DICOM format for the specific implementation and may be taken from 512×512 up to 64×64. In addition, the pixels values of the DICOM images are transformed to gray images; mean they are standardized to [0, 1].

B. PERFORMANCE METRIC

For the performance metric of the methods as a reconstruction quality, the signal-to-noise ratio (SNR) and structural similarity index (SSIM) is opted in this paper.

The SNR is determined as:

$$\mathrm{SNR} = 20\log_{10}\left(\frac{\|s\|_2}{\|s-\hat{s}\|_2}\right), \tag{7}$$

where s and $\hat{s}$ indicates the original images and reconstructed images.

The SSIM is a perceptual metric that reflects the quality deterioration produced by data compression or by losses in data transmission is given as:

$$\mathrm{SSIM(x,\,y)} = [\mathrm{l(x,\,y)}]^{\alpha} \cdot [\mathrm{c(x,\,y)}]^{\beta} \cdot [\mathrm{s(x,\,y)}]^{\gamma}, \tag{8}$$

where

$$\begin{aligned} \mathrm{l(x,\,y)} &= \frac{2\mu_{\mathrm{x}}\mu_{\mathrm{y}} + \mathrm{C}o}{\mu_{\mathrm{x}}^2 + \mu_{\mathrm{y}}^2 + \mathrm{C}_o}, \\ \mathrm{c(x,\,y)} &= \frac{2\sigma_{\mathrm{x}}\sigma_{\mathrm{y}} + \mathrm{C}_p}{\sigma_{\mathrm{x}}^2 + \sigma_{\mathrm{y}}^2 + \mathrm{C}_p}, \\ \mathrm{s(x,\,y)} &= \frac{\sigma_{\mathrm{xy}} + \mathrm{C}_q}{\sigma_{\mathrm{x}}\sigma_{\mathrm{y}} + \mathrm{C}_q}, \end{aligned} \tag{9}$$

where μ_x and μ_y are the local means, σ_x and σ_y are standard deviations, and σ_{xy} is cross-covariance for CT images x, y.

If C_q is used as default, $\mathrm{C}_q = \mathrm{C}_p/2$, and $\alpha = \beta = \gamma = 1$ is set for exponents, the SSIM interprets to:

$$\mathrm{SSIM(x,\,y)} = \frac{\left(2\mu_{\mathrm{x}}\mu_{\mathrm{y}} + \mathrm{C}_o\right)\left(2\sigma_{\mathrm{xy}} + \mathrm{C}_p\right)}{\left(\mu_{\mathrm{x}}^2 + \mu_{\mathrm{y}}^2 + \mathrm{C}_o\right)\left(\sigma_{\mathrm{x}}^2 + \sigma_{\mathrm{y}}^2 + \mathrm{C}_p\right)}. \tag{10}$$

V. RESULT

This section evaluates the proposed technique by comparing with SARA, reweighted Haar (RW-Haar), and reweighted curvelet (RW-Curvelet), in terms of SNR, SSIM, and processing time. The ratio of (M) and (N) is the most critical variable and $\frac{M}{N} \leq 0.5$ denotes sampling ratio under Nyquist rate. Therefore, the simulation condition is defined as follows: the sampling ratio ($\frac{M}{N}$) number is [0.1, 0.2, . . . , 0.5], the maximum number of iterations of the reweighted algorithm is 10, the minimum relative change in the solution is 10^{-3}, $L = 4$ is used for the wavelet level decomposition, and Daubechies type.

A. SNR RESULT

The SNR of the reconstructed images is calculated using (7) and evaluated for the proposed technique, SARA, RW-Haar, and RW-Curvelet. The SNR results are presented in box plot and shown in Fig. 3 for 100 CT images. The red line in box plot denotes median, the lower edge of the blue box denotes 25th percentile, the upper edge of the blue box denotes 75th percentile, and the black dashed line denotes upper and lower adjacent of the SNR results. The X-value of the figure corresponding four different method (Proposed, SARA, RW-Haar, RW-Curv.) and Y-value is the SNR results. The proposed technique outperforms all existing CS techniques with higher median result in box plot at all $\frac{M}{N}$ setting as presented in Fig. 3.

Fig. 3(a) show the highest adjacent at SNR = 50.86 dB for the proposed technique and the lowest adjacent at SNR = 5.99 dB for RW-Haar. The proposed technique outperforms SARA, RW-Haar, and RW-Curvelet in median, maximum, 25%, 75%, lower adjacent, and upper adjacent of 100 SNR results. For lower adjacent of SNR results, the proposed technique achieves SNR = 11.85 dB and SARA achieves SNR = 10.85 dB, where the proposed technique outperforms SARA with the SNR gap is 1 dB in the box plot. The upper adjacent of the proposed technique is 52.25 dB and the upper adjacent of SARA is 51.24 dB, where the different of the upper adjacent result is 1.01 dB. For 25th percentile of SNR results, 16.23 dB and 15.37 dB are achieved by the proposed technique and SARA, respectively. For 75th percentile of SNR results, 47.49 dB is achieved by the proposed technique and SARA achieves 46.23 dB. Clearly, the proposed technique outperform all method with higher SNR at $\frac{M}{N} = 0.1$.

From Fig. 3(b), the highest adjacent at SNR = 60.55 dB is achieved by the proposed technique and the lowest adjacent at SNR = 12.41 dB is achieved by RW-Curvelet. Clearly, the proposed technique outperforms SARA, RW-Haar, and RW-Curvelet, in terms of median, upper adjacent, lower adjacent, 25th percentile, 75th percentile of the SNR results. For the lower adjacent of SNR results, the proposed technique achieves SNR = 20.15 dB, SARA achieves SNR = 19.21 dB, RW-Haar achieves SNR = 13.53 dB, and RW-Curvelet achieves SNR = 12.41 dB in the box plot. The upper adjacent of the proposed technique, SARA, RW-Haar, and RW-Curvelet are 60.55 dB, 57.76 dB, 49.27 dB, and 50.70 dB, respectively. For 25th percentile of SNR results, 27.52 dB is achieved by the proposed technique, 26.20 dB is achieved by SARA, 18.46 dB is achieved by RW-Haar, and 15.92 dB is achieved by RW-Curvelet. For 75th percentile of SNR results, the proposed technique achieves 56.55 dB, SARA achieves 52.134 dB, RW-Haar achieves 37.76 dB, and RW-Curvelet achieves 46.80 dB. The proposed technique outperforms all CS techniques with higher SNR at $\frac{M}{N} = 0.3$.

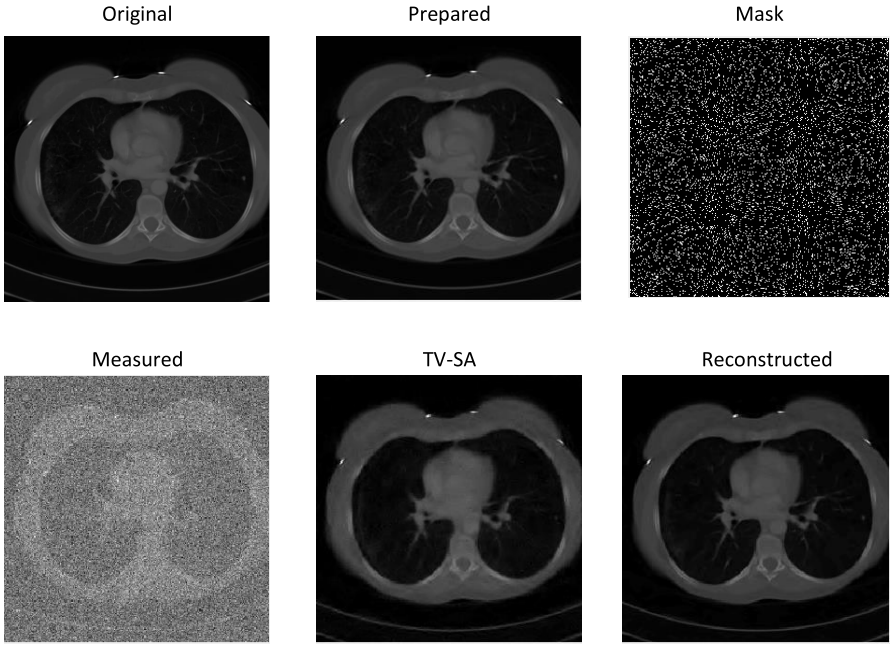

FIGURE 2. An example of CT images. First, original image is processed to prepared image. Second, mask is used to measure the prepared images for measured image. Third, measured image is reconstructed using TV based SA method. Last, the result from TV-SA is perform reweighted TV to get reconstructed image.

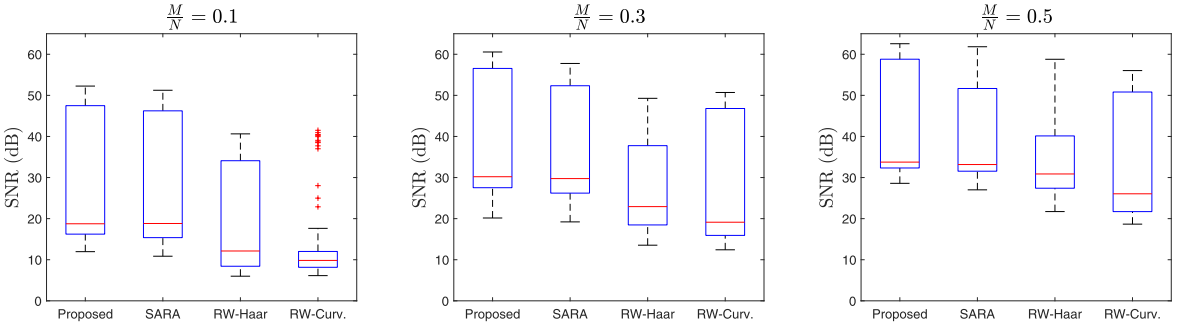

FIGURE 3. Box plot of SNR results. (a) $\frac{M}{N} = 0.1$. (b) $\frac{M}{N} = 0.3$. (c) $\frac{M}{N} = 0.5$.

From Fig. 3(c), the proposed technique achieves the highest SNR = 62.56 dB and outperform SARA, where the lowest SNR = 18.66 dB is achieved by RW-Curvelet. Clearly, the proposed technique outperform SARA in terms of median, upper adjacent, lower adjacent, 25th percentile, 75 percentile of the SNR results. For median, the proposed technique achieves 33.75 dB, SARA achieves 33.16 dB, RW-Haar achieves 30.87 dB, and RW-Curvelet achieves 26.04 dB. For 25th percentile of SNR results, 32.32 dB is achieved by the proposed technique, 31.54 dB is achieved by SARA, 27.40 dB is achieved by RW-Haar, and 21.71 dB is achieved by RW-Curvelet. For 75th percentile of SNR results, the proposed technique achieves 58.79 dB, SARA achieves 51.67 dB, RW-Haar achieves 40.13 dB, and RW-Curvelet achieves 50.81 dB. The lower adjacent of the proposed technique is 28.59 dB, SARA is 27.01 dB, RW-Haar is 21.72 dB, and RW-Curvelet is 18.66 dB. The upper adjacent of the proposed technique, SARA, RW-Haar, and RW-Curvelet are 62.56 dB, 61.83 dB, 58.78 dB, and 56.03 dB, respectively.

In addition, Table. 1 and Fig. 4 present the detailed of average SNR results for measurement ratio $\frac{M}{N} = [0.1, \ldots, 0.5]$. Table 1 also presents the $\pm$ denotes the standard deviation of the 100 SNR results for 100 CT images. Fig. 4 shows the proposed technique achieves the best average SNR result.

B. SSIM RESULT

The SSIM of the reconstructed images using the proposed technique, SARA, RW-Haar, and RW-Curvelet are evaluated

TABLE 1. Comparison of average SNR measures between different measurement rate.

Measurement ratio $\left(\frac{M}{N}\right)$	Proposed	SARA	RW-Haar	RW-Curvelet
0.1	27.3902 ± 14.8646	26.7388 ± 14.6833	18.5106 ± 12.5836	13.1568 ± 9.4971
0.2	33.8192 ± 14.6601	32.6792 ± 14.0225	22.751 ± 11.1116	23.9361 ± 14.9297
0.3	37.9731 ± 14.0717	36.0051 ± 12.6215	27.5189 ± 10.5901	27.4069 ± 14.6092
0.4	40.2981 ± 13.4471	38.2702 ± 11.8751	29.9375 ± 7.555	29.9478 ± 13.6144
0.5	41.6848 ± 12.9256	39.2796 ± 10.6228	33.6507 ± 8.2296	33.0277 ± 13.6865

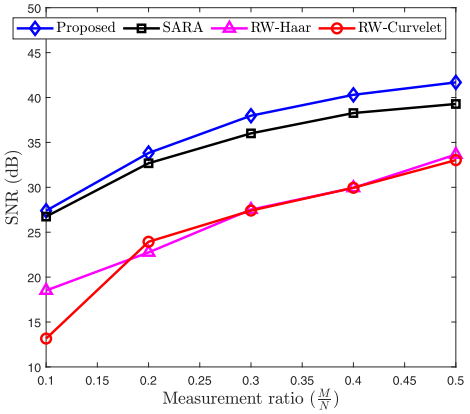

FIGURE 4. Average SNR results.

according to (10). Fig. 5 shows the box plot of SSIM results for 100 CT images, where a red line is median, a lower edge blue box is 25th percentile, and the upper edge of the blue box is 75th percentile of the 100 SSIM results. The Y-value is the SSIM results and the X-value is the four different method (Proposed, SARA, RW-Haar, RW-Curvelet).

Fig. 5(a) show SSIM results for $\frac{M}{N} = 0.1$ with the highest adjacent value (SSIM $= 0.9957$) is achieved by the proposed technique and the lowest adjacent value (SSIM $= 0.01$ at the outlier value) is achieved by RW-Curvelet. For RW-Curvelet, 26 finite outliers are appeared, lower adjacent is 0.1528, 25h percentile is 0.3696, median is 0.4400, 75th percentile is 0.5295, and upper adjacent is 0.6510. For RW-Haar, lower adjacent is 0.3115, the 25th percentile is 0.3940, the median is 0.4831, the 75th percentile is 0.8665, and the upper adjacent is 0.9593. For SARA, the lower adjacent is 0.6310, the 25th percentile is 0.7554, the median is 0.8270, the 75th percentile is 0.9837, and the upper adjacent is 0.9947. For the proposed technique, the lower adjacent is 0.6874, the 25th percentile is 0.7691, the median is 0.8379, the 75th percentile is 0.9880, and the upper adjacent is 0.9957.

Fig. 5(b) show SSIM results for $\frac{M}{N} = 0.3$ with the highest adjacent value (SSIM $= 0.9993$) is achieved by the proposed technique and the lowest adjacent value (SSIM $= 0.6404$) is achieved by RW-curvelet. For RW-Curvelet, 25th percentile is 0.7342, median is 0.8104, 75th percentile is 0.9840, and upper adjacent is 0.9937. For RW-Haar, lower adjacent is 0.7289, the 25th percentile is 0.8301, the median is 0.8945, the 75th percentile is 0.9334, and the upper adjacent is 0.9922. For SARA, the lower adjacent is 0.9165, the 25th percentile is 0.9617, the median is 0.973, the 75th percentile is 0.9956, and the upper adjacent is 0.9986. For the proposed technique, the lower adjacent is 0.9352, the 25th percentile is 0.9726, the median is 0.9809, the 75th percentile is 0.9983, and the upper adjacent is 0.9993.

From Fig. 5(c), RW-TV achieves the highest SSIM $=$ 0.9995 and outperform SARA, same result also for TV compared to BPSA. For RW-Curvelet, lower adjacent is 0.8269, 25h percentile is 0.8963, median is 0.9278, 75th percentile is 0.9933, and upper adjacent is 0.9981. For RW-Haar, a finite outlier is appeared, lower adjacent is 0.9148, the 25th percentile is 0.9524, the median is 0.9672, the 75th percentile is 0.9786, and the upper adjacent is 0.9989. For SARA method, the lower adjacent is 0.9701, the 25th percentile is 0.9843, the median is 0.9872, the 75th percentile is 0.9948, and the upper adjacent is 0.9994. For the proposed technique, the lower adjacent is 0.9734, the 25th percentile is 0.9885, the median is 0.9909, the 75th percentile is 0.9989, and the upper adjacent is 0.9995.

In comparison, Table 2 presents average SSIM results for measurement ratio $\frac{M}{N} = [0.1, \ldots, 0.5]$ with the $\pm$ denotes the standard deviation of the 100 SSIM results for 100 CT images. The proposed technique outperforms SARA with higher median result in box plot at all $\frac{M}{N}$ setting.

C. PROCESSING TIME RESULT

The processing time of the reconstructed images is evaluated for the proposed technique, SARA, RW-Haar, and RW-Curvelet. The processing time result of 100 CT images are presented in box plot and shown in Fig. 7. The median is denoted by red line in box plot, the 25th percentile is denoted by the lower edge of the blue box, and the 75th percentile is denoted by the upper edge of the blue box. The X-value of the figure corresponding four different method (Proposed, SARA, RW-Haar, RW-Curvelet) and Y-value is the processing time in seconds. The proposed technique outperforms SARA, RW-Haar, and RW-Curvelet at all $\frac{M}{N}$ setting which is presented in Fig. 7.

Fig. 7(a) presents processing time for $\frac{M}{N} = 0.1$ with the highest adjacent value is 45.04 seconds for RW-Curvelet and the lowest adjacent value is 0.1359 seconds for RW-Haar. For the proposed technique, six finite outliers are appeared, the lower adjacent is 0.391 seconds, the 25th percentile is 0.840 seconds, the median is 1.060 seconds, the 75th percentile is 2.340 seconds, and the upper adjacent is 4.187 seconds. For SARA, the lower adjacent is 2.118 seconds, the 25th percentile is 6.732 seconds, the median is

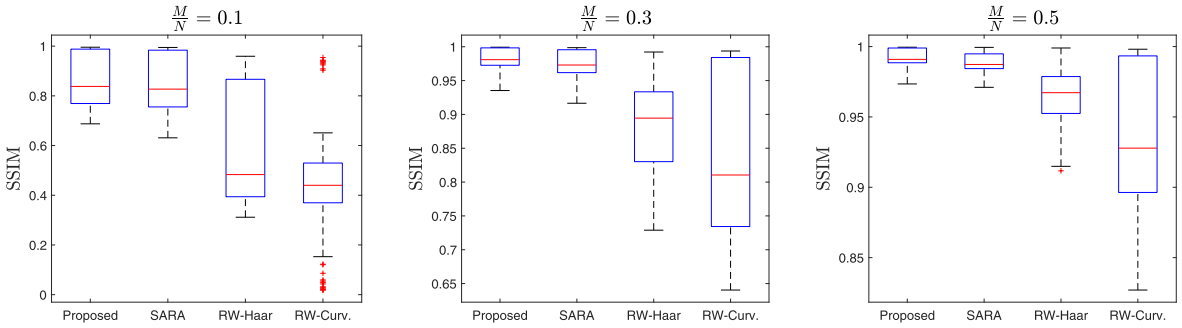

FIGURE 5. Box plot of SSIM results. (a) $\frac{M}{N} = 0.1$. (b) $\frac{M}{N} = 0.3$. (c) $\frac{M}{N} = 0.5$.

TABLE 2. Comparison of average SSIM measures between different measurement rate.

Measurement ratio $\left(\frac{M}{N}\right)$	Proposed	SARA	RW-Haar	RW-Curvelet
0.1	0.85875 ± 0.10255	0.84655 ± 0.112	0.58517 ± 0.22787	0.43481 ± 0.23866
0.2	0.95535 ± 0.038514	0.94536 ± 0.044445	0.75965 ± 0.12919	0.74507 ± 0.1723
0.3	0.98159 ± 0.015321	0.9741 ± 0.019287	0.88301 ± 0.067332	0.83726 ± 0.11701
0.4	0.98922 ± 0.0081533	0.98438 ± 0.010168	0.93238 ± 0.029674	0.89725 ± 0.075154
0.5	0.9923 ± 0.0056414	0.98862 ± 0.0063845	0.96401 ± 0.019688	0.93658 ± 0.047575

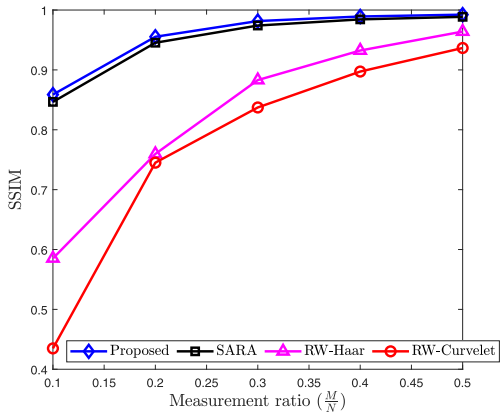

FIGURE 6. Average SSIM results.

7.646 seconds, the 75th percentile is 10.074 seconds, and the upper adjacent is 13.6385 seconds. For RW-Haar, lower adjacent is 0.1359 seconds, 25h percentile is 0.4387 seconds, median is 8.3696 seconds, 75th percentile is 10.328 seconds, and upper adjacent is 14.443 seconds. For RW-Curvelet, lower adjacent is 4.4276 seconds, the 25th percentile is 8.0753 seconds, the median is 9.8907 seconds, the 75th percentile is 17.7065 seconds, and the upper adjacent is 30.4884 seconds.

Processing time for $\frac{M}{N} = 0.3$ is shown on Fig. 7(b), where the highest adjacent value with 17.712 seconds is achieved by SARA and the lowest adjacent value with 0.0927 seconds is achieved by RW-Haar. For the proposed technique, ten finite outliers are appeared, the lower adjacent is 0.430 seconds, the 25th percentile is 0.739 seconds, the median is 0.964 seconds, the 75th percentile is 1.912 seconds, and the upper adjacent is 3.664 seconds. For SARA method, the lower adjacent is 1.135 seconds, the 25th percentile is 6.464 seconds, the median is 8.066 seconds, the 75th percentile is 10.995 seconds, and the upper adjacent is 17.712 seconds. For RW-Haar, lower adjacent is 0.0927 seconds, 25h percentile is 3.859 seconds, median is 8.868 seconds, 75th percentile is 10.1361 seconds, and upper adjacent is 12.766 seconds. For RW-Curvelet, 14 finite outliers are appeared, lower adjacent is 1.5773 seconds, the 25th percentile is 4.0038 seconds, the median is 5.0709 seconds, the 75th percentile is 5.6471 seconds, and the upper adjacent is 7.4639 seconds.

Fig. 7(c) show processing time for $\frac{M}{N} = 0.5$ with the highest adjacent value is 32.650 seconds for SARA and the lowest adjacent value is 0.08348 seconds for RW-Haar. For the proposed technique, ten finite outliers are appeared, the lower adjacent is 0.462 seconds, the 25th percentile is 0.652 seconds, the median is 0.846 seconds, the 75th percentile is 1.170 seconds, and the upper adjacent is 1.937 seconds. For SARA method, four finite outliers are appeared, the lower adjacent is 3.827 seconds, the 25th percentile is 5.380 seconds, the median is 6.601 seconds, the 75th percentile is 10.257 seconds, and the upper adjacent is 17.509 seconds. For RW-Haar, lower adjacent is 0.08348 seconds, 25h percentile is 0.15982 seconds, median is 7.2454 seconds, 75th percentile is 8.41 seconds, and upper adjacent is 10.8935 seconds. For BRW-Curvelet, lower adjacent is 0.4804 seconds, the 25th percentile is 2.403 seconds, the median is 3.908 seconds, the 75th percentile is 4.4311 seconds, and the upper adjacent is 6.409 seconds.

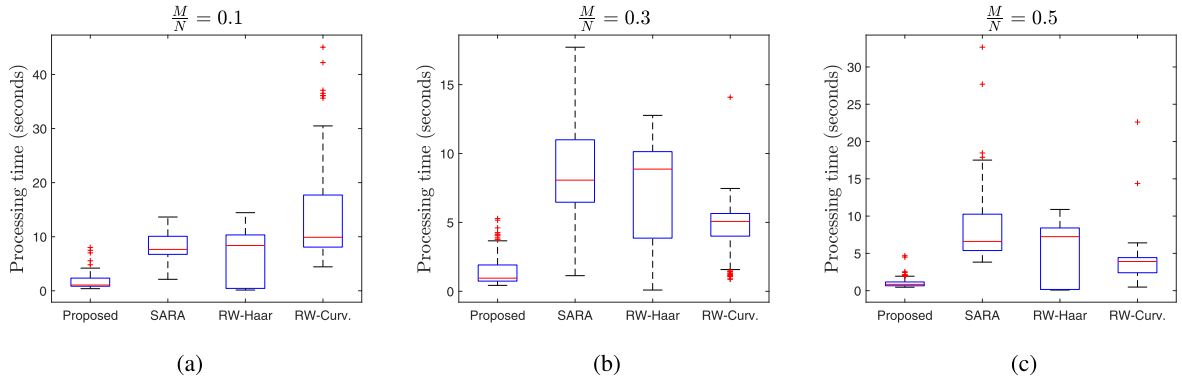

FIGURE 7. Box plot of processing time results. (a) Measurement ratio = 0.1. (b) Measurement ratio = 0.3. (c) Measurement ratio = 0.5.

TABLE 3. Comparison of average processing time with regards to measurement ratio.

Measurement ratio $\left(\frac{M}{N}\right)$	Proposed	SARA	RW-Haar	RW-Curvelet
0.1	1.7708 ± 1.5044	8.4008 ± 2.109	6.6126 ± 4.47	14.1553 ± 9.3946
0.2	1.6213 ± 1.2966	9.1613 ± 3.4742	6.9313 ± 4.5713	6.3136 ± 2.2798
0.3	1.5195 ± 1.1996	9.0149 ± 3.5749	7.0783 ± 4.1419	4.6177 ± 1.9062
0.4	1.3127 ± 0.92505	10.0641 ± 4.6304	5.8984 ± 4.1538	3.5275 ± 1.8291
0.5	1.0572 ± 0.69225	8.4888 ± 4.7182	5.701 ± 3.6379	3.7327 ± 2.7286

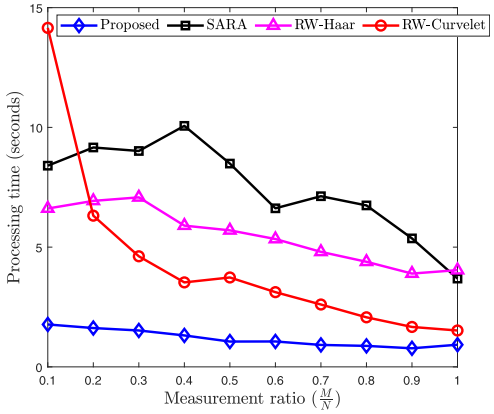

FIGURE 8. Average processing time results for RW-TV and SARA.

In comparison, Table 3 present average processing time for measurement ratio $\frac{M}{N} = [0.1, \ldots, 0.5]$ in detail with the $\pm$ denotes the standard deviation of the 100 results for 100 CT images.

D. THE EFFECT OF IMAGE RESOLUTIONS

The effect of image resolutions is evaluated for the proposed technique, SARA, RW-Haar, and RW-Curvelet. The SNR result of 100 CT images are presented in bar plot and shown in Fig. 9. The X-value of the figure corresponding three different resolutions (64×64 pixels, 128×128 pixels, and 256×256 pixels) and Y-value is SNR in dB.

Fig. 9(a) presents SNR results with regards to resolutions for $\frac{M}{N} = 0.1$ with the best result is 37.64 dB achieved by SARA with 256×256 pixels and the lowest result is 13.15 dB achieved by RW-Curvelet with 64×64 pixels. For resolution 64×64 pixels, the proposed technique outperforms SARA, RW-Haar, and RW-Curvelet with 0.66 dB, 8.88 dB, and 14.24 dB higher, respectively. For resolution 128×128 pixels, the SNR of the proposed technique is 32.22 dB, the SNR of SARA is 32.02 dB, the SNR of RW-Haar is 22.33 dB, and RW-Curvelet is 22.01 dB. For resolution 256×256 pixels, SARA achieves the best SNR result (37.60 dB), the proposed technique achieves 36.12 dB, RW-Haar achieves 26.77 dB, and RW-Curvelet achieves 25.76 dB.

SNR results with regards to image resolutions for $\frac{M}{N} = 0.3$ is shown on Fig. 9(b), where the best result SNR (42.69 dB) is achieved by the proposed technique with 256×256 pixels and the lowest SNR result (27.40 dB) is achieved by RW-Curvelet with 64×64 pixels. The proposed technique achieves 37.97 dB, 40.72 dB, and 42.69 dB for resolutions 64×64 pixels, 128×128 pixels, and 256×256 pixels, respectively. The proposed technique outperforms SARA, RW-Haar, and RW-Curvelet in all resolution conditions.

Fig. 9(c) presents SNR results with regards to resolutions for $\frac{M}{N} = 0.5$ with the best result is 44.61 dB achieved by the proposed technique with 256×256 pixels and the lowest results is 33.02 dB for RW-Curvelet with 64×64 pixels. For resolution 64×64 pixels, the proposed technique (41.68 dB) outperforms SARA (39.27 dB), RW-Haar (33.65 dB), and RW-Curvelet (33.02 dB) with 2.41 dB, 8.03 dB, and 8.66 dB, respectively. For resolution 128×128 pixels, the SNR of the proposed technique is 43.55 dB, the SNR of SARA is 41.33 dB, the SNR of RW-Haar is 38.20 dB, and RW-Curvelet is 36.17 dB. For resolution 256×256 pixels, the proposed technique achieves the best SNR result (44.61 dB),

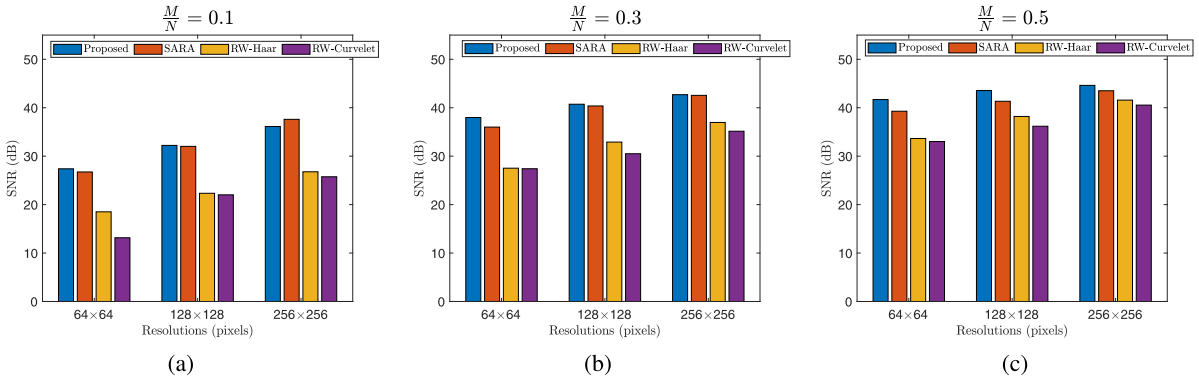

FIGURE 9. SNR results with regards to image resolutions. (a) Measurement ratio = 0.1. (b) Measurement ratio = 0.3. (c) Measurement ratio = 0.5.

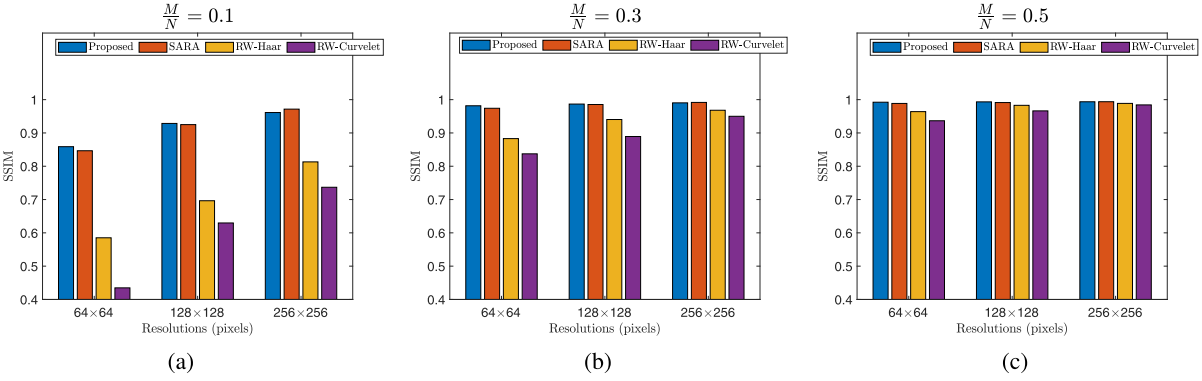

FIGURE 10. SSIM results with regards to image resolutions. (a) Measurement ratio = 0.1. (b) Measurement ratio = 0.3. (c) Measurement ratio = 0.5.

SARA achieves 43.50 dB, RW-Haar achieves 41.57 dB, and RW-Curvelet achieves 40.54 dB.

Next, the SSIM result of 100 CT images with regards to image resolutions are presented in bar plot and shown in Fig. 10. The X-value of the figure corresponding three different resolutions (64 × 64 pixels, 128 × 128 pixels, and 256 × 256 pixels) and Y-value is SSIM.

Fig. 10(a) presents SSIM results with regards to resolutions for $\frac{M}{N} = 0.1$ with the best result is 0.9715 for SARA with 256×256 pixels and the lowest result is 0.43 for RW-Curvelet with 64 × 64 pixels. For resolution 64 × 64 pixels, the SSIM of the proposed technique is 0.8587, the SSIM of SARA is 0.8465, the SSIM of RW-Haar is 0.5851, and RW-Curvelet is 0.4348. For resolution 128 × 128 pixels, the SSIM of the proposed technique is 0.9285, the SSIM of SARA is 0.9250, the SSIM of RW-Haar is 0.6964, and RW-Curvelet is 0.6296. For resolution 256 × 256 pixels, the SSIM of the proposed technique is 0.9613, the SSIM of SARA is 0.9715, the SSIM of RW-Haar is 0.8130, and RW-Curvelet is 0.7369.

SSIM results with regards to image resolutions for $\frac{M}{N} = 0.3$ is shown on Fig. 10(b), where the best result SSIM (0.9903) is achieved by the proposed technique with 256 × 256 pixels and the lowest SNR result (0.8372) is achieved by RW-Curvelet with 64 × 64 pixels. The proposed technique achieves 0.9815, 0.9867, and 0.9903 for resolutions 64 × 64 pixels, 128 × 128 pixels, and 256 × 256 pixels, respectively. The proposed technique outperforms SARA, RW-Haar, and RW-Curvelet in all resolution conditions.

Fig. 10(c) presents SSIM results with regards to resolutions for $\frac{M}{N} = 0.5$ with the best result is 0.9936 achieved by the proposed technique with 256 × 256 pixels and the lowest results is 9365 achieved by RW-Curvelet with 64 × 64 pixels. For resolution 64 × 64 pixels, the proposed technique achieves 0.9923,SARA achieves 0.9886, RW-Haar achieves 0.9640, and RW-Curvelet achieves 0.9365. For resolution 128 × 128 pixels, the SSIM of the proposed technique is 0.9933, the SSIM of SARA is 0.9912, the SSIM of RW-Haar is 0.9829, and RW-Curvelet is 0.9662. For resolution 256 × 256 pixels, the proposed technique achieves 0.9936, SARA achieves the best SSIM result with result 0.9937, RW-Haar achieves 0.9887, and RW-Curvelet achieves 0.9841.

Finally, the processing time result of 100 CT images are presented in bar plot and shown in Fig. 11. The X-value of the figure corresponding three different resolutions (64 × 64 pixels, 128 × 128 pixels, and 256 × 256 pixels) and Y-value is processing time in seconds.

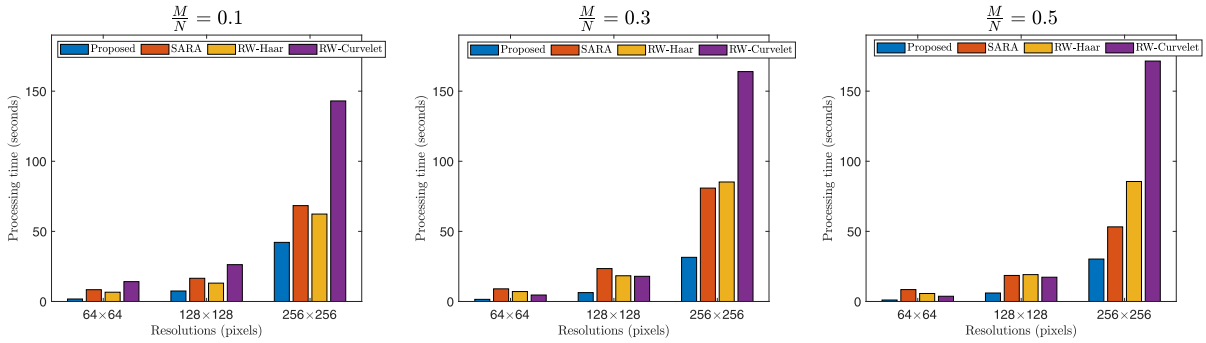

FIGURE 11. Processing time results with regards to image resolutions. (a) Measurement ratio = 0.1. (b) Measurement ratio = 0.3. (c) Measurement ratio = 0.5.

Fig. 11(a) presents the processing time results with regards to resolutions for $\frac{M}{N} = 0.1$ with the best result is 1.770 seconds achieved by the proposed technique with 64×64 pixels and the longest processing time result is 143.026 seconds for RW-Curvelet with 256×256 pixels. For resolution 64×64 pixels, the processing time of the proposed technique is 1.770 seconds, the processing time of SARA is 8.4 seconds, the processing time of RW-Haar is 6.612 seconds, and RW-Curvelet is 14.115 seconds. For resolution 128×128 pixels, the processing time of the proposed technique, SARA, RW-Haar, and RW-Curvelet is 7.479 seconds, 16.55 seconds, 13.091 seconds, and 26.268 seconds, respectively. For resolution 256×256 pixels, the result of the proposed technique is 42.15 seconds, SARA is 68.36 seconds, RW-Haar is 62.34 seconds, and RW-Curvelet is 143.02 seconds.

Fig. 11(b) presents the processing time results with regards to resolutions for $\frac{M}{N} = 0.3$ with the best result is 1.519 seconds achieved by the proposed technique with 64×64 pixels and the longest processing time result is 163.956 seconds for RW-Curvelet with 256×256 pixels. For resolution 64×64 pixels, the processing time of the proposed technique is 1.519 seconds, the processing time of SARA is 9.014 seconds, the processing time of RW-Haar is 7.078 seconds, and RW-Curvelet is 4.617 seconds. For resolution 128×128 pixels, the processing time of the proposed technique, SARA, RW-Haar, and RW-Curvelet is 6.332 seconds, 23.468 seconds, 18.344 seconds, and 17.951 seconds, respectively. For resolution 256×256 pixels, the result of the proposed technique is 31.49 seconds, SARA is 80.87 seconds, RW-Haar is 85.21 seconds, and RW-Curvelet is 163.95 seconds.

Fig. 11(c) presents the processing time results with regards to resolutions for $\frac{M}{N} = 0.5$ with the best result is 1.05 seconds achieved by the proposed technique with 64×64 pixels and the longest processing time result is 171.47 seconds for RW-Curvelet with 256×256 pixels. For resolution 64×64 pixels, the processing time of the proposed technique is 1.05 seconds, the processing time of SARA is 8.4 seconds, the processing time of RW-Haar is 5.7 seconds, and RW-Curvelet is 3.7 seconds. For resolution 128×128 pixels, the processing time of the proposed technique, SARA, RW-Haar, and RW-Curvelet is 6.046 seconds, 18.569 seconds, 19.159 seconds, and 17.311 seconds, respectively. For resolution 256×256 pixels, the result of the proposed technique is 43.026 seconds, SARA is 53.21 seconds, RW-Haar is 85.58 seconds, and RW-Curvelet is 171.47 seconds.

VI. CONCLUSION

In this paper, TV based average sparsity model with reweighted analysis is proposed for computed tomography (CT) image compression. The proposed CS technique is evaluated and compared to existing CS technique (e.g., SARA, RW-Haar, RW-Curvelet) by evaluating the SNR, SSIM, and processing time. Enlightened by the better SNR, the proposed technique outperforms SARA, RW-Haar, RW-Curvelet with 1.5 dB, 8.8 dB, 14.24 dB, respectively. For SSIM results at measurement ratio 0.1, the proposed technique outperforms SARA with 0.01 improvement, outperforms RW-Haar with 0.3 improvement, outperforms RW-Curvelet with 0.42 improvement. And in the same testing parameter for 64×64 pixels of CT images, the processing time of the proposed technique is 6.7 seconds faster than SARA, 4.9 seconds faster than RW-Haar, and 12.4 seconds faster than RW-Curvelet. In this way, the proposed technique has better SNR with lower processing time, which is considers as a feasible solution for compressed sensing (CS) based CT images compression with faster delay process and better visual quality for medical images.

REFERENCES

[1] H. Kong, X. Lei, L. Lei, Y. Zhang, and H. Yu, "Spectral CT reconstruction based on PICCS and dictionary learning," *IEEE Access*, vol. 8, pp. 133367–133376, 2020.

[2] Z. Shen, C. Gong, W. Yu, and L. Zeng, "Guided image filtering reconstruction based on total variation and prior image for limited-angle CT," *IEEE Access*, vol. 8, pp. 151878–151887, 2020.

[3] T. W. Cabral, M. Khosravy, F. M. Dias, H. L. M. Monteiro, M. A. A. Lima, L. R. M. Silva, R. Naji, and C. A. Duque, "Compressive sensing in medical signal processing and imaging systems," in *Sensors for Health Monitoring* (Advances in Ubiquitous Sensing Applications for Healthcare), vol. 5, N. Dey, J. Chaki, and R. Kumar, Eds. New York, NY, USA: Academic, 2019, ch. 4, pp. 69–92. [Online]. Available: https://www.sciencedirect.com/science/article/pii/B978012819361700004X

[4] D. L. Donoho, "Compressed sensing," *IEEE Trans. Inf. Theory*, vol. 52, no. 4, pp. 1289–1306, Apr. 2006.
[5] E. J. Candès and T. Tao, "Near-optimal signal recovery from random projections: Universal encoding strategies?" *IEEE Trans. Inf. Theory*, vol. 52, no. 12, pp. 5406–5425, Dec. 2006.
[6] E. J. Candès and M. B. Wakin, "An introduction to compressive sampling," *IEEE Signal Process. Mag.*, vol. 25, no. 2, pp. 21–30, Mar. 2008.
[7] L. Wang, L. Li, L. Jin, L. Jing, B. B. Gupta, and L. Xia, "Compressive sensing of medical images with confidentially homomorphic aggregations," *IEEE Internet Things J.*, vol. 6, no. 2, pp. 1402–1409, Apr. 2019.
[8] M. Jacob, J. C. Ye, L. Ying, and M. Doneva, "Computational MRI: Compressive sensing and beyond [from the guest editors]," *IEEE Signal Process. Mag.*, vol. 37, no. 1, pp. 21–23, Jan. 2020.
[9] C. G. Graff and E. Y. Sidky, "Compressive sensing in medical imaging," *Appl. Opt.*, vol. 54, no. 8, pp. C23–C44, 2015.
[10] R. E. Carrillo, J. D. McEwen, D. Van De Ville, J.-P. Thiran, and Y. Wiaux, "Sparsity averaging for compressive imaging," *IEEE Signal Process. Lett.*, vol. 20, no. 6, pp. 591–594, Jun. 2013.
[11] T. Rahim, L. Novamizanti, I. N. A. Ramatryana, and S. Y. Shin, "Compressed medical imaging based on average sparsity model and reweighted analysis of multiple basis pursuit," *Comput. Med. Imag. Graph.*, vol. 90, Jun. 2021, Art. no. 101927. [Online]. Available: https://www.sciencedirect.com/science/article/pii/S0895611121000768
[12] G.-H. Chen, J. Tang, and S. Leng, "Prior image constrained compressed sensing (PICCS): A method to accurately reconstruct dynamic CT images from highly undersampled projection data sets," *Med. Phys.*, vol. 35, no. 2, pp. 660–663, 2008.
[13] Z. Zhu, K. Wahid, P. Babyn, D. Cooper, I. Pratt, and Y. Carter, "Improved compressed sensing-based algorithm for sparse-view CT image reconstruction," *Comput. Math. Methods Med.*, vol. 2013, pp. 1–15, Mar. 2013.
[14] X. Li and S. Luo, "A compressed sensing-based iterative algorithm for CT reconstruction and its possible application to phase contrast imaging," *Biomed. Eng. OnLine*, vol. 10, no. 1, p. 73, 2011.
[15] A. Perelli, M. Lexa, A. Can, and M. E. Davies, "Compressive computed tomography reconstruction through denoising approximate message passing," *SIAM J. Imag. Sci.*, vol. 13, no. 4, pp. 1860–1897, Jan. 2020.
[16] E. Y. Sidky and X. Pan, "Image reconstruction in circular cone-beam computed tomography by constrained, total-variation minimization," *Phys. Med. Biol.*, vol. 53, no. 17, p. 4777, 2008.
[17] Z. Qu, X. Yan, J. Pan, and P. Chen, "Sparse view CT image reconstruction based on total variation and wavelet frame regularization," *IEEE Access*, vol. 8, pp. 57400–57413, 2020.
[18] N. Khanna, V. Kumar, and S. K. Kaushik, "Wavelet packet approximation," *Integral Transforms Special Functions*, vol. 27, no. 9, pp. 698–714, 2016.
[19] N. Khanna, S. K. Kaushik, and A. M. Jarrah, "Wavelet packets: Uniform approximation and numerical integration," *Int. J. Wavelets, Multiresolution Inf. Process.*, vol. 18, no. 2, Mar. 2020, Art. no. 2050004.
[20] Q. Guo, Y. Li, X. Liang, J. Dong, and R. Cheng, "Through-the-Wall image reconstruction via reweighted total variation and prior information in radio tomographic imaging," *IEEE Access*, vol. 8, pp. 40057–40066, 2020.
[21] Y. Chen, J. Liu, L. Xie, Y. Hu, H. Shu, L. Luo, L. Zhang, Z. Gui, and G. Coatrieux, "Discriminative prior–prior image constrained compressed sensing reconstruction for low-dose CT imaging," *Sci. Rep.*, vol. 7, no. 1, pp. 1–17, Dec. 2017.
[22] S. Hashemi, S. Beheshti, P. R. Gill, N. S. Paul, and R. S. C. Cobbold, "Accelerated compressed sensing based CT image reconstruction," *Comput. Math. Methods Med.*, vol. 2015, pp. 1–16, May 2015.
[23] H. Zanddizari, D. Mitra, and S. Rajan, "Blind deterministic compressive sensing for biomedical images," in *Proc. IEEE Int. Symp. Med. Meas. Appl. (MeMeA)*, Jun. 2020, pp. 1–5.
[24] H. Mohimani, M. Babaie-Zadeh, and C. Jutten, "A fast approach for overcomplete sparse decomposition based on smoothed ℓ^o norm," *IEEE Trans. Signal Process.*, vol. 57, no. 1, pp. 289–301, Jan. 2009.
[25] P. Hanumanth, P. Bhavana, and S. Subbarayappa, "Application of deep learning and compressed sensing for reconstruction of images," *J. Phys., Conf. Ser.*, vol. 1706, Dec. 2020, Art. no. 012068.
[26] Y. Yang, J. Sun, H. Li, and Z. Xu, "ADMM-CSNet: A deep learning approach for image compressive sensing," *IEEE Trans. Pattern Anal. Mach. Intell.* vol. 42, no. 3, pp. 521–538, Mar. 2020.
[27] T. N. Canh and B. Jeon, "Multi-scale deep compressive imaging," *IEEE Trans. Comput. Imag.*, vol. 7, pp. 86–97, 2021.
[28] C. Gan, X. Yan, Y. Wu, and Z. Zhang, "A two-branch convolution residual network for image compressive sensing," *IEEE Access*, vol. 8, pp. 1705–1714, 2020.
[29] M. Mardani, E. Gong, J. Y. Cheng, S. S. Vasanawala, G. Zaharchuk, L. Xing, and J. M. Pauly, "Deep generative adversarial neural networks for compressive sensing MRI," *IEEE Trans. Med. Imag.*, vol. 38, no. 1, pp. 167–179, Jan. 2019.
[30] Z. Yuan, M. Jiang, Y. Wang, B. Wei, Y. Li, P. Wang, W. Menpes-Smith, Z. Niu, and G. Yang, "SARA-GAN: Self-attention and relative average discriminator based generative adversarial networks for fast compressed sensing MRI reconstruction," *Frontiers Neuroinform.*, vol. 14, Nov. 2020, Art. no. 611666.
[31] R. E. Carrillo, J. D. McEwen, and Y. Wiaux, "Sparsity averaging reweighted analysis (SARA): A novel algorithm for radio-interferometric imaging," *Monthly Notices Roy. Astron. Soc.*, vol. 426, no. 2, pp. 1223–1234, 2012.
[32] G. Puy, P. Vandergheynst, R. Gribonval, and Y. Wiaux, "Universal and efficient compressed sensing by spread spectrum and application to realistic Fourier imaging techniques," *EURASIP J. Adv. Signal Process.*, vol. 2012, no. 1, pp. 1–13, Dec. 2012.
[33] H. Rauhut, K. Schnass, and P. Vandergheynst, "Compressed sensing and redundant dictionaries," *IEEE Trans. Inf. Theory*, vol. 54, no. 5, pp. 2210–2219, Apr. 2008.
[34] E. J. Candès, Y. C. Eldar, D. Needell, and P. Randall, "Compressed sensing with coherent and redundant dictionaries," *Appl. Comput. Harmon. Anal.*, vol. 31, no. 1, pp. 59–73, Jul. 2011.
[35] R. Giryes, S. Nam, M. Elad, R. Gribonval, and M. E. Davies, "Greedy-like algorithms for the cosparse analysis model," *Linear Algebra Appl.*, vol. 441, pp. 22–60, Jan. 2014.
[36] R. Gribonval and M. Nielsen, "Sparse representations in unions of bases," *IEEE Trans. Inf. Theory*, vol. 49, no. 12, pp. 3320–3325, Dec. 2003.
[37] J. Bobin, J.-L. Starck, J. M. Fadili, Y. Moudden, and D. L. Donoho, "Morphological component analysis: An adaptive thresholding strategy," *IEEE Trans. Image Process.*, vol. 16, no. 11, pp. 2675–2681, Nov. 2007.
[38] S. Dabiri, K. Popuri, E. M. Cespedes Feliciano, B. J. Caan, V. E. Baracos, and M. F. Beg, "Muscle segmentation in axial computed tomography (CT) images at the lumbar (L3) and thoracic (T4) levels for body composition analysis," *Comput. Med. Imag. Graph.*, vol. 75, pp. 47–55, Jul. 2019.

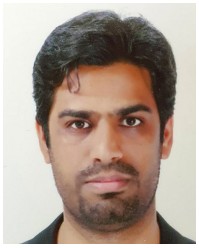

TARIQ RAHIM (Member, IEEE) received the B.Sc. degree from the COMSAT Institute of Information and Technology, Pakistan, the M.S. degree from Beijing Institute of Technology, China, and the Ph.D. degree in IT convergence engineering from the Wireless and Emerging Network System Laboratory (WENS Lab), Kumoh National Institute of Technology (KIT), South Korea. He is currently working as a Postdoctoral Fellow and a Researcher at ICT-CRC, KIT, South Korea. His research interests include signal processing, image processing, medical image analysis, deep learning, video processing, and quality of services of high frame rate videos.

LEDYA NOVAMIZANTI (Graduate Student Member, IEEE) received the Bachelor of Science (S.Si.) degree in mathematics from Andalas University, Indonesia, in 2005, and the Master of Engineering (M.T.) degree in electrical engineering from Telkom University, Indonesia, in 2018. She has been working as a Lecturer with Telkom University, since 2010. Her current research interests include signal processing, computer vision, pattern recognition, and artificial intelligence.

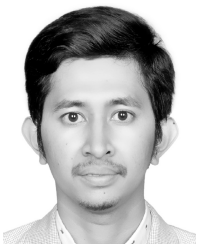

I NYOMAN APRAZ RAMATRYANA (Graduate Student Member, IEEE) received the bachelor's degree in telecommunication engineering and the master's degree in electrical and telecommunication engineering from the Telkom Institute of Technology (currently known as Telkom University), Indonesia, in 2010 and 2014, respectively. He is currently pursuing the Ph.D. degree in IT convergence engineering with the Kumoh National Institute of Technology, South Korea. His areas of expertise are signal processing, artificial intelligence (AI), wireless communications, and computer vision. His research interests include random access (RA), raptor coding, non-orthogonal multiple access (NOMA), multiple-input multiple-output (MIMO) antenna, compressed imaging, medical imaging, and deep learning (DL).

SOO YOUNG SHIN (Senior Member, IEEE) received the B.S., M.S., and Ph.D. degrees in electrical engineering and computer science from Seoul National University, South Korea, in 1999, 2001, and 2006, respectively. He was a Visiting Scholar with the FUN Laboratory, University of Washington, USA, from July 2006 to June 2007. After three years of working with the WiMAX Design Laboratory, Samsung Electronics, he has been an Associate Professor with the School of Electronics, Kumoh National Institute of Technology, since September 2010. His research interests include wireless LAN, WPAN, WBAN, wireless mesh networks, sensor networks, coexistence among wireless networks, industrial and military networks, cognitive radio networks, and next generation mobile wireless broadband networks.

DONG SEONG KIM (Senior Member, IEEE) received the Ph.D. degree in electrical and computer engineering from Seoul National University, Seoul, South Korea, in 2003. From 1994 to 2003, he worked as a full-time Researcher with ERC-ACI, Seoul National University. From March 2003 to February 2005, he worked as a Postdoctoral Researcher with the Wireless Network Laboratory, School of Electrical and Computer Engineering, Cornell University, NY, USA. From 2007 to 2009, he was a Visiting Professor with the Department of Computer Science, University of California at Davis, Davis, CA, USA. He is currently the Director of the KIT Convergence Research Institute and the ICT Convergence Research Center (ITRC and NRF advanced research center program) supported by the Korean Government, Kumoh National Institute of Technology. His current research interests include the real-time IoT and smart platform, industrial wireless control networks, networked embedded systems, and Fieldbus. He is a Senior Member of ACM.